

Research Report

Novel Genetic and Biochemical Insights into the Spectrum of *NEFL*-Associated Phenotypes

Adela Della Marina^a, Andreas Hentschel^b, Artur Czech^b, Ulrike Schara-Schmidt^a, Corinna Preusse^c, Andreas Laner^d, Angela Abicht^{d,e}, Tobias Ruck^f, Joachim Weis^g, Catherine Choueiri^h, Hanns Lochmüller^{h,i,j}, Heike Kölbel^{a,1} and Andreas Roos^{a,f,h,*,1}

^aDepartment of Pediatric Neurology, Centre for Neuromuscular Disorders, Centre for Translational Neuro- and Behavioral Sciences, University Duisburg-Essen, Essen, Germany

^bLeibniz-Institut für Analytische Wissenschaften -ISAS- e.V., Dortmund, Germany

^cCharité-Universitätsmedizin Berlin, Corporate Member of Freie Universität Berlin, Humboldt-Universität zu Berlin, and Berlin Institute of Health (BIH), Berlin, Germany

^dMedical Genetics Center, Munich, Germany

^eFriedrich-Baur Institute, Ludwig Maximilian University, Munich, Germany

^fDepartment of Neurology, Medical Faculty, Heinrich Heine University Düsseldorf, Düsseldorf, Germany

^gInstitute of Neuropathology, RWTH Aachen University Hospital, Aachen, Germany

^hChildren's Hospital of Eastern Ontario Research Institute, Ottawa, ON, Canada

ⁱDivision of Neurology, Department of Medicine, The Ottawa Hospital, Ottawa, Canada

^jBrain and Mind Research Institute, University of Ottawa, Ottawa, Canada

Accepted 6 March 2024

Pre-press 3 April 2024

Published 30 April 2024

Abstract.

Background: *NEFL* encodes for the neurofilament light chain protein. Pathogenic variants in *NEFL* cause demyelinating, axonal and intermediate forms of Charcot-Marie-Tooth disease (CMT) which present with a varying degree of severity and somatic mutations have not been described yet. Currently, 34 different CMT-causing pathogenic variants in *NEFL* in 174 patients have been reported. Muscular involvement was also described in CMT2E patients mostly as a secondary effect. Also, there are a few descriptions of a primary muscle vulnerability upon pathogenic *NEFL* variants.

Objectives: To expand the current knowledge on the genetic landscape, clinical presentation and muscle involvement in *NEFL*-related neurological diseases by retrospective case study and literature review.

Methods: We applied in-depth phenotyping of new and already reported cases, molecular genetic testing, light-, electron- and Coherent Anti-Stokes Raman Scattering-microscopic studies and proteomic profiling in addition to *in silico* modelling of *NEFL*-variants.

Results: We report on a boy with a muscular phenotype (weakness, myalgia and cramps, Z-band alterations and minicores in some myofibers) associated with the heterozygous p.(Phe104Val) *NEFL*-variant, which was previously described in a neuropathy case. Skeletal muscle proteomics findings indicated affection of cytoskeletal proteins. Moreover, we report on two further neuropathic patients (16 years old girl and her father) both carrying the heterozygous p.(Pro8Ser) variant, which has been identified as 15% somatic mosaic in the father. While the daughter presented with altered neurophysiology,

¹Shared last authorship.

*Correspondence to: PD Dr Andreas Roos. Tel.: +49 201 723 2165; Fax: +49 201 723 5389. E-mail: andreas.roos@uk-essen.de.

neurogenic clump feet and gait disturbances, the father showed clinically only feet deformities. As missense variants affecting proline at amino acid position 8 are leading to neuropathic manifestations of different severities, *in silico* modelling of these different amino acid substitutions indicated variable pathogenic impact correlating with disease onset.

Conclusions: Our findings provide new morphological and biochemical insights into the vulnerability of denervated muscle (upon NEFL-associated neuropathy) as well as novel genetic findings expanding the current knowledge on NEFL-related neuromuscular phenotypes and their clinical manifestations. Along this line, our data show that even subtle expression of somatic *NEFL* variants can lead to neuromuscular symptoms.

Keywords: Neurofilament light chain, protein accumulation, muscle proteomics, somatic mutation, CARS microscopy muscle

INTRODUCTION

Neurofilament light chain (NEFL) protein is one of the neurofilament-core-subunits, forming heterodimers. Neurofilaments (NFL) provide structural stability to neurons. They are essential for the radial growth of axons during development, the expansion and maintenance of axonal caliber, and the transmission of electrical impulses on axons [1, 2]. NEFL proteins are subunits of neurofilaments in both the central and the peripheral nervous system and as such, dysfunction of the NEFL protein could give rise to pathology in either of the two parts of the nervous system [3]. Toxic neurofilament-accumulation is a hallmark of many neurodegenerative disorders like autoimmune-mediated motor neuron injury [4], amyotrophic lateral sclerosis (ALS) [5], Charcot-Marie-Tooth disease, 5q-related spinal muscular atrophy (SMA), spastic paraplegia, Alzheimer's disease and Parkinson's disease [6].

Charcot-Marie-Tooth (CMT) has been classified electrophysiologically into three major phenotypes: predominantly demyelinating forms (CMT1), predominantly axonal forms (CMT2) and dominant-intermediate forms [2]. Pathogenic *NEFL* variants may cause demyelinating (CMT1F), axonal (CMT2E) and dominant intermediate forms (DICMTG). Hereby, the disease-associated variants are located throughout the functional domains of the protein, which associates with subunits of the “medium” (NEFM) and the “heavy” (NEFH) protein versions to form coiled-coil dimers resulting in the build-up of 10 nm sized intermediate filaments [11].

Currently, more than 30 different CMT-causing pathogenic variants in *NEFL* have been reported, which embrace the head, rod, and tail domains of the protein. Most of the mutations are dominant missense variants functioning through a gain-of-function mechanism by perturbing neurofilament assembly and organelle transport in axons [12]. Only

three autosomal recessive nonsense mutations were reported with associated severe, early-onset phenotypes [13–15]. However, current phenotype-genotype correlations suggest a loss-of-function mechanism due to the lack of NF networks for bi-allelic variants whereas the impact of the different dominant variants on respective phenotypical manifestations are still not completely understood [2, 16, 17]. Further studies in a primary motor neuron culture model indicated that mitochondrial dysfunction contributes to the pathogenesis of CMT2E [18]. This might be one of the reasons for the presence of additional, non-neuropathic symptoms including hereditary spastic paraplegia, progressive spasticity, intellectual impairment and hearing loss in some of the patients [16, 19–21]. Muscular involvement is described as a clinical feature in CMT2E patients mostly recognized as a secondary effect but overlapping myopathic findings and clinical features of a congenital myopathy were described in some cases [17]. Increased creatine kinase (CK) levels and additional myopathic changes including myofiber size variation, rounding of fibers, ring fibers, and nemaline bodies in muscle biopsies of CMT2E patients are a further hint towards a concomitant muscular effect of pathogenic *NEFL* variants [22]. These descriptions accord with the results of functional studies obtained in a porcine model of muscle development, showing that expression of *NEFL* plays a significant role in embryonic morphogenesis and skeletal muscle development [23].

Interestingly, pathogenic variants affecting other genes (such as *LMNA*, *DNM2* and *BAG3*) are associated with the manifestation of diseases across the neuromuscular axis and may cause myopathy or neuropathy [24, 25]. This phenomenon may be related to disruption of different tissue-specific functions of the respective proteins [26]. However, studies focusing on *NEFL*-based myopathological changes in human muscle tissue are still rare.

PATIENTS, MATERIALS AND METHODS

Patients

Patients included in this study were phenotyped in the Department of Pediatric Neurology of the University Hospital of Essen (Duisburg-Essen University). Written informed consent for clinical description, genetic studies, and utilization of the muscle biopsy for research purposes was obtained from the patients' parents. The study was conducted according to the guidelines of the Declaration of Helsinki and approved by the Ethics Committee of University of Duisburg-Essen (19-9011-BO).

Molecular genetic studies

Genomic DNA was obtained from total peripheral blood samples using routine extraction methods. Next-generation sequencing (gene panel analysis including 1.678 genes with relevance in clinical diagnostics, custom-made target enrichment, Agilent Sure Select) was carried out on an Illumina NextSeq 500 system (Illumina, San Diego, CA) as 150 bp paired-end runs using v2.0 SBS chemistry. Sequencing reads were aligned to the human reference genome (GRCh37/hg19) using BWA (v0.7.13-r1126) with standard parameters. Statistics on coverage and sequencing depth on the clinical targeted regions (i.e. RefSeq coding exons and ± 5 intronic region) were calculated with a custom script. SNV and INDEL calling on the nuclear genes was conducted using SAMtools (v1.3.1) with subsequent coverage and quality dependent filter steps. Variant annotation was performed with snpEff (v4.2) and Alamut-Batch (v1.4.4). Only variants (SNVs/small INDELS) in the coding and flanking intronic regions (± 50 bp) were evaluated. BayesDel (<https://fenglab.chpc.utah.edu/BayesDel/BayesDel.html>) and the thresholds published by Pejaver et al. [27] were used for bioinformatic predictions. Variants were classified according to the ACMG (American College of Medical Genetics and genomics) guidelines taking the current recommendations from ClinGen's Sequence Variant Interpretation Working Group (SVI) into account [16, 28] and classifying variants with the 5-tier classification system: class 5 (pathogenic), class 4 (likely pathogenic), class 3 (uncertain variants or variants of unknown significance, VUS), class 2 (likely not pathogenic) and class 1 (not pathogenic).

In silico modelling of amino acid substitutions affecting Pro 8

ColabFold version 1.5.2 was employed using the AlphaFold2_mmseqs2 Jupyter notebook to predict the three-dimensional structures of the wild-type NEFL protein (UniProt accession: P07196) and five missense NEFL protein variants [29]. Each three-dimensional structure was predicted alongside pLDDT score, which is a per-residue confidence metric between 1–100 generated by AlphaFold2 [30]. PyMOL was then used to individually superimpose the wild-type NEFL protein model onto each of the missense protein variant models using the "super" command. The "super" command also computes a root-mean-square deviation (rmsd) score for each superimposition, representing structural similarity between the two models [31]. Finally, the predicted protein models were uploaded to PremPS, a web server that can be used to predict the effects of missense mutations on protein stability, measured by unfolding free energy change ($\Delta\Delta G$) [32]. The five NEFL missense mutations were specified to the PremPS server, and the changes in non-covalent interactions between wild-type NEFL and each missense variant were modelled, exclusively focusing on non-covalent interactions between the mutated amino acid residue and its adjacent residues. A $\Delta\Delta G$ value (kcal/mol) was estimated for each mutation as an indicator of protein stability change as a result of the mutation, with positive and negative $\Delta\Delta G$ values indicating mutations that either destabilize or stabilize the protein structure, respectively [32].

Biopsy work-up

Muscle biopsy specimen investigated in this study (from patient 1) has initially been collected for diagnostic purposes including histology, enzyme histochemistry, immunofluorescence and immunohistochemical investigations. Serial cryosections (7 μm) of transversely-oriented muscle blocks were stained according to standard procedures with hematoxylin and eosin (H&E), Gömöri trichrome (GT), oil red, COX-SDH and SDH and nicotinamide adenine dinucleotide tetrazolium reductase (NADH-TR) [33]. Microscopy was performed using a Zeiss Axio-plan epifluorescence microscope and a Zeiss Axio Cam ICc 1.

Glutaraldehyde-fixed specimens were processed for ultrastructural examination by standard procedures. The tissue was post-fixed in 1% osmium

tetroxide and embedded in Epon 812. Semithin sections for light microscopy were stained with toluidine blue. Ultrathin sections were contrasted with uranyl acetate and lead citrate and examined using a Philips CM10 transmission electron microscope as described [34].

Coherent anti-Stokes Raman scattering microscopy (CARS)

From a cyro-preserved muscle biopsy specimen, 5 μm sections were prepared and used for coherent anti-Stokes Raman scattering (CARS) as well as for second harmonic generation (SHG) microscopy. Samples were dried in a nitrogen stream and required no further sample preparation.

For the CARS/SHG measurements, a modified Leica TCS SP 8 CARS was used with an APE picoEmerald as the laser source (as described previously, [35]). CARS and SHG signals were detected simultaneously in backward (Epi; E) and in forward (F) direction. For the imaging, we used a 40 \times water immersion objective lens (IRAPO 40 \times /1.10 WATER). For imaging and acquisition of CARS spectra, a field of 291 \times 291 μm (2048 \times 2048 pixels) was measured on the samples. By tuning the pump laser from 804.0 nm to 826.4 nm with a step size of 0.7 nm, a pixel dwell time of approximately 10 μs and averaging of two images, we acquired the FCARS spectra.

Statistical evaluation of muscle fibre calibres

Length and width of fully imaged muscle fibres were manually measured from merged FCARS/ESHG images utilizing the Leica software Las X. The muscle fibre calibre was averaged from the two lengths. For muscle fibres in longitudinal orientation, width of the fibres was determined as the calibre. For this purpose, a total of 6 images of the patient and 8 images of the disease control were analysed.

Acquisition of the spectra of the feature findings

The spectral CARS/SHG measurements were manually screened for conspicuous features. These were grouped according to their appearance (see results section). The CARS spectra in each group were first normalized and then averaged. For comparison, inconspicuous areas neighbouring the features (BG) were handled alike. A total of 194 spectra were used for the spectra presented in the results section: pBG: 45, pProt: 45, dcBG: 69, dcProt: 11, dcLip: 24, cBG: 135.

Proteomic profiling

Proteomic profiling of whole muscle protein extracts was carried out as described previously in a data-independent-acquisition mode [36].

RESULTS

Clinical findings

Patient 1: was born as the first child of non-consanguineous parents of German origin. Pregnancy and birth were uneventful. At the age of 1.5 years, developmental language problems occurred, sensorineural hearing loss was diagnosed and linked to the compound-heterozygous *CX26* (*GJB2*) variants c.109G>A, p.(Val37Ile) (ClinGen Hearing Loss Expert Panel Curation classified as “pathogenic”) and c.100_101delinsCC, p.(Met34Pro) (classified as “likely pathogenic”) using ACMG-AMP codes PM5, PM3, PM1, PM2_SUP). However, motor milestones were achieved in time. Due to cognitive impairment (IQ: 64) and behavioral problems (both are not part of the phenotypic spectrum associated with variants in *CX26*) a basic diagnostic work-up (echocardiography, electrocardiogram [ECG], laboratory values including basic laboratory examinations for metabolic disorders as well as a screening for congenital disorders of glycosylation (CDG) was performed with normal results. Karyotype was 46, XY. Electroencephalography (EEG) at 24 months of age showed no pathological findings, brain and spine magnetic resonance imaging (MRI) revealed normal findings. At the age of 2 years, muscle cramps and muscular stiffness of lower extremities (especially in the morning) as the first signs of a neuromuscular involvement occurred. Creatine kinase (CK) was slightly elevated (210 U/l; norm < 149 U/l). Muscle biopsy was performed at the age of 6 years assuming a muscular disease. Phenotyping at his last visit (at the age of 11 years) revealed reduced endurance (walking distance < 300 m), muscle cramps under muscular strain accompanied by slowly progressing gait disturbances, hyperlordosis, normal reflex levels for patellar tendon reflex (PTR) and absent achilles tendon reflex (ATR), pes cavus, small CMAP, marginally reduced nerve conduction velocities (NCV) and prolonged distal latencies (Fig. 1).

Patient 2: was born as the first child of non-consanguineous parents of German origin. She was preterm born at 28 weeks of gestation due to cardiac failure of the mother under resuscitation. Mother

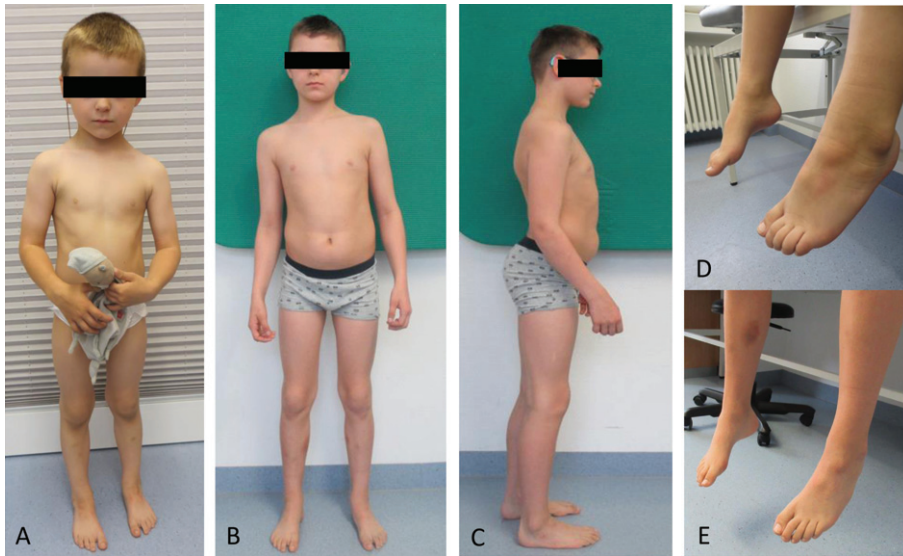


Fig. 1. Clinical findings in one *NEFL*-patient. Patient 1 at the age of 3 years (A and D) and 11 years (B, C and E). Note lack of progress in pes cavus within the period of 7 years. Hyperlordosis at the age of 11 years (C).

deceased during delivery. After 10 weeks of hospitalization the infant was discharged with need of tube feeding for 3 months. She had intraventricular bleeding one sided due to prematurity (ultrasound). MRI of brain at the age of 11 years was normal. Persistent ductus arteriosus and atrial septum defect were operated during infancy. Her motor milestones were slightly delayed; she was able to walk unsupported at the age of 21 months, but falls were frequent. Speech and cognitive development were age appropriate. At the age of 5 years, the patient developed an abnormal gait pattern with unstable gait, with inward positions of the knee and the development of pes cavus. She had reduced proximal muscle strength and could stand up from the sitting position only with support. She had problems to open a bottle due to distal muscle weakness. This new symptom could not be explained as a consequence of premature birth and thus further diagnostic was initiated. The basic work-up (echocardiography, electrocardiogram [ECG], laboratory values including CK and basic laboratory examinations for metabolic disorders as well as electroencephalography [EEG], brain and spine MRI) revealed normal findings. At the age of 11 years, the patient underwent surgery for feet deformity including heel cord lengthening. Her clinical findings at her last visit (at the age of 16 years) revealed reduced walking distance (approximately 1200 m), brisk reflex levels, sensory ataxia, pes cavus, small CMAP, reduced NCV and prolonged

distal latencies in her arms (Nervus (N) medianus and N. ulnaris, sensible and motoric) and absent in legs (motoric and sensible NCV not reproducible) (patient 7 in Table 1).

Father of patient 2: He reported pes cavus at both feet since early infancy/childhood (exact age of onset not known) without any progression, no reduced endurance or gait disturbances. His father had also pes cavus as far as he can remember. Last neurological examination at the age of 47 years showed normal results for his muscular strength and muscular tonus with brief muscle reflexes in his upper extremities and PTR, but reduced reflexes at ATR. Nerve conduction velocity studies revealed prolonged distal latencies (6.0/6.3 m/sec) and slightly reduced motor NCV (40/37 m/sec) at both N. peroneus as a mild neuropathic sign (patient 8 in Table 1).

Molecular genetic findings

Patient 1: By next generation sequencing we identified the heterozygous variant c.310T>G; p.(Phe104Val) in the *NEFL* gene (NM 006158.4). The nucleotide substitution from T to G at position 310 leads to a predicted amino acid exchange from phenylalanine to valine. The corresponding amino acids show minor differences in polarity, charge and size (Grantham dist.: 50 [0–215]). The amino acid phenylalanine at position 104 is located in the “intermediate filament protein” domain of the *NEFL*

Table 1

Summary of clinical, molecular genetic and in silico prediction based findings in patient harbouring amino acid substitutions affection position 8 (modified based on Jordanova et al 2003 [38]). Overview of the clinical and neurophysiological data from patients harbouring mutations in codon 8 of NEFL reported in the literature including our patients [14, 16, 56, 57]. In silico modelling results estimated either stabilising or destabilising $\Delta\Delta G$ values for the five NEFL variants. NCV – nerve conduction velocity, LE – lower extremity, UE – upper extremity, ND – not determined, ATR – Achilles tendon reflex

	Jordanova et al., 2003						This study	
	Family				Singleton	Singleton	Family	
	Patient 1	Patient 2	Patient 3	Patient 4	Patient 5	Patient 6	Patient 7	Patient 8
Pathogenic variant	c.23C>G; p.(Pro8Arg)	c.23C>G; p.(Pro8Arg)	c.23C>G; p.(Pro8Arg)	c.23C>G; p.(Pro8Arg)	c.23C>A; p.(Pro8Gln)	c.23C>T; p.(Pro8Leu)	c.22C>T; p.(Pro8Ser)	c.22C>T; p.(Pro8Ser) (mosaic)
<i>In silico</i> modelling	2.551	2.551	2.551	2.551	2.928	7.959	2.924	
Rmsd	0.18	0.18	0.18	0.18	0.26	-0.39 (stabilizing)	-0.11 (stabilizing)	
$\Delta\Delta G$ [kcal/mol]G	(destabilizing)	(destabilizing)	(destabilizing)	(destabilizing)	(destabilizing)			
Age of onset (years)	7	11	12	13	5	<2	4	Early childhood (exact age not determined)
Initial symptoms	ND	Gait problems	ND	ND	ND	Delayed walking	Frequent fall	none
Clinical -neuromuscular symptoms	Muscle weakness UE and LE, muscle atrophy, areflexia, Pes cavus	Muscle weakness LE, muscle atrophy UE and LE, diminished deep tendon reflexes, Pes cavus	Muscle weakness LE, Muscle atrophy UE and LE, sensory loss, diminished deep tendon reflexes, Pes cavus	Muscle weakness LE, muscle atrophy UE and LE, sensory loss, Pes cavus	Muscle weakness UE and LE, sensory loss, diminished relaxes, Pes cavus	Muscle weakness UE and LE, areflexia, Pes cavus	Muscle weakness LE, Pes cavus, distal weakness UE	Pes cavus, reduced ATR reflexes
Sensory loss	yes	yes	Yes	yes	yes	ND	yes	no
Additional symptoms	Joint contractures	Tremor, dysphagia	none	none	Contractures of lower limbs	Tremor	Preterm born 28 weeks	none
Motor development	ND	ND	ND	ND	ND	delayed	Light delayed, walking 21 months	Normal
Mental development	Not tested	Not tested	Not tested	Not tested	Partial learning deficits	Not tested (regular school)	Normal	Normal
Age at last follow up	35 years	65 years	42 years	39 years	30 years	30 years	16 years	47 years
NCV (m/s)	N. medianus 38 N. ulnaris 47 N. peroneus 17	ND	ND	ND	N. medianus 21 N. ulnaris 33 N. peroneus ND	N. medianus 27 N. ulnaris 19 N. peroneus 23	N. medianus reduced N. ulnaris reduced N. peroneus (no conduction)	N. peroneus 37

	Miltenberger-Milteneu et al., 2007							Abe et al., 2009	Lin et al., 2011		Horga et al., 2018
	Family							Singleton	Singleton	Singleton	Singleton
	Patient 9	Patient 10	Patient 11	Patient 12	Patient 13	Patient 14	Patient 15	Patient 16	Patient 17	Patient 18	Patient 19
Pathogenic variant	c.23C>G (Pro8Arg)	c.23 C>G (Pro8Arg)	c.23C>G (Pro8Arg)	c.23C>G (Pro8Arg)	c.23C>G [Pro8Arg]	c.23C>G (Pro8Arg)	c.23C>G (Pro8Arg)	c.23C>T (Pro8Leu)	c.23C>G (Pro8Arg)	c.23C>G (Pro8Arg)	c.23C>G (Pro8Arg)
In silico modelling Rmsd $\Delta\Delta G$ [kcal/mol]G	2.551 0.18 (destabilizing)	2.551 0.18 (destabilizing)	2.551 0.18 (destabilizing)	2.551 0.18 (destabilizing)	2.551 0.18 (destabilizing)	2.551 0.18 (destabilizing)	2.551 0.18 (destabilizing)	7.959 -0.39 (stabilizing)	2.551 0.18 (destabilizing)	2.551 0.18 (destabilizing)	2.551 0.18 (destabilizing)
Age of onset (years)	12	15	12	25	13	ND	8	<10	10	10	Second decade
Initial symptoms	Unsteady gait	Gait problems	Unsteady gait	Gait problems	Unsteady gait	Unsteady gait	Foot deformity	Gait problems	ND	ND	Restless leg, unsteady gait, tremor
Clinical-neuromuscular symptoms	Muscle weakness UE and LE, muscle atrophy, areflexia, Pes cavus	Muscle weakness UE and LE, muscle atrophy, areflexia, Pes cavus	Muscle weakness UE and LE, muscle atrophy, areflexia, Pes cavus	Muscle weakness LE, muscle atrophy UE and LE, sensory loss, Pes cavus	Muscle weakness UE and LE, muscle atrophy, areflexia, Pes cavus	Muscle weakness UE and LE, muscle atrophy, areflexia	Muscle weakness UE and LE, muscle atrophy, areflexia, Pes cavus	Muscle weakness UE and LE, muscle atrophy, areflexia, Pes cavus	ND	ND	Muscle weakness LE and UE, areflexia,
Sensory los	yes	yes	ND	yes	yes	yes	yes	yes	ND	ND	yes
Additional symptoms	Hyperlordosis	Cerebellar signs	Kyphoscoliosis	Fasciculations	Ataxia, tremor	Schizophrenia		Joint contractures	ND	ND	Head tremor, restless leg syndrome, periodic limb movement disorder
Motor development	ND	ND	ND	ND	ND	ND	ND	Normal	ND	ND	ND
Mental development	ND	Not tested	Not tested	Not tested				Normal	ND	ND	Not tested
Last follow up (age)	49 years	77 years	71 years	61 years	51 years	50 years	29 years	27 years	26 years	47 years	53 years
NCV (m/s) Single nervs	ND	N. medianus 40.8 N. ulnaris 48.7	N. medianus 38.2 N. ulnaris 37.8	ND	ND	ND	N. medianus 23	N medianus 33	N. medianus 40.8 N. ulnaris 48.7	N. medianus 38.2, N. ulnaris 37.8	N. medianus 38.2 N. ulnaris 37.8

protein and is highly conserved across many species. The absence of this variant in population-specific databases can be considered as supporting evidence for a pathogenic effect. This variant has been detected in one individual from a cohort of patients with peripheral neuropathy [37]. Bioinformatic prediction using BayesDel suggest a strong pathogenic effect. The result of the family analysis suggests a *de novo* origin of the sequence variant in the index patient, supporting a pathogenic effect of the variant. According to the ACMG-guidelines [28], the variant was classified as “likely pathogenic” (evidence codes: PS4_SUP, PM2_SUP, PM6_SUP, PP3_Strong).

Patient 2: We identified the heterozygous variant c.22C>T; p.(Pro8Ser) in the *NEFL* gene. This variant has not yet been described in the literature, but three other amino acid exchanges at the same codon have been described as being pathogenic (c.23C>G; p.(Pro8Arg); c.23C>A; p.(Pro8Gln) & c.23C>T; p.(Pro8Leu)) [38], indicating that the proline at this amino acid position is critical for NEFL protein activity. Assumed pathogenicity of the variant is not only suggested by the biochemical nature (substitution of a neutral-polar but non-circular amino acid (Ser) to a polar circular one (Pro)) but was also supported by segregation analysis: A targeted Sanger sequencing revealed that the variant c.22C>T; p.(Pro8Ser) could be detected in the mildly affected father as a low-grade somatic mosaic (about 15% in peripheral blood). Additionally, this variant has been detected in a confirmed *de novo* constellation in a Taiwanese CMT-patient [39] and has moreover been described in at least two unrelated individuals with NEFL-associated phenotypes (ClinVar VCV000576990.5). However, in case of this one reported individual, the authors do not provide any data supporting pathogenicity and therefore we have at least included this “evidence” under PS4 (proband counting). Taken together, this variant was classified as “likely pathogenic” (evidence codes: PS2_MOD, PS4_SUP, PM2_SUP, PM5), according to the ACMG guidelines and following the recent recommendation from ClinGen’s Sequence Variante Interpretation Working Group (<https://clinicalgenome.org/working-groups/sequence-variant-interpretation/>).

In silico modelling of amino acid substitutions affecting proline at position 8

To address the impact of the nature of amino acid substitutions on the manifestation of clinical symp-

toms in terms of severity of phenotypes associated with different missense variants affecting amino acid position 8, AlphaFold2-based *in silico* studies were carried out: the six NEFL protein structures were predicted with pLDDT scores ranging from 71.8–72.4 (Fig. 5A). When superimposed onto the wild-type NEFL protein model, the Phe104Val and Pro8Leu protein variants exhibited rmsd scores of 4.739 Å and 7.959 Å, respectively, which were the highest rmsd scores among the modelled variants (Fig. 5B & Table 1). On the other hand, Pro8Ser, Pro8Gln, and Pro8Arg exhibited rmsd scores between 2.5 Å and 3.0 Å when superimposed onto wild-type NEFL (Fig. 5B & Table 1). Identical structures are indicated by a rmsd of 0 Å, a rmsd up to 2.0 Å reflects good structural similarity, and a rmsd of 3.0 Å and above indicates low similarity [40–42]

PremPS predicted that all five variants alter the hydrophobic interactions between the mutated and its adjacent residues (Fig. 5C). The p.(Phe104Val) variant introduces a new hydrophobic interaction between Val104 and Val108. The Pro8Ser variant lacks all three hydrophobic interactions between Pro8 and Tyr6 that are present in wild-type NEFL. Pro8Arg leads to the loss of a hydrophobic interaction between Arg8 and Tyr6, and p.(Pro8Gln) leads to the loss of a hydrophobic interaction between Gln8 and Tyr6. Lastly, the p.(Pro8Leu) mutation causes one hydrophobic interaction to be lost between Leu8 and Tyr6 while also introducing two new hydrophobic interactions between Leu8 and Tyr10. All changes in hydrophobic interactions were associated with a $\Delta\Delta G$ value (kcal/mol) (Table 1). PremPS estimated either stabilising or destabilising $\Delta\Delta G$ values for the five NEFL variants. Both stabilising and destabilising $\Delta\Delta G$ values have been associated with deleterious mutations. The Pro8Leu variant showed a $\Delta\Delta G$ of -0.35 kcal/mol compared to wild-type NEFL, which was the highest magnitude $\Delta\Delta G$ value among the variants tested. Thus, our *in silico* predictions underline the pathogenic character of the amino acid substitution identified in our NEFL-patients and moreover demonstrate that missense variants affecting the same amino acid substitution may have diverging deleterious effects in terms of irregular stabilization or destabilization of NEFL.

Histological and electron microscopic findings on NEFL-mutant muscle

Histological examination did not reveal striking myopathic changes in the patient 1’s muscle

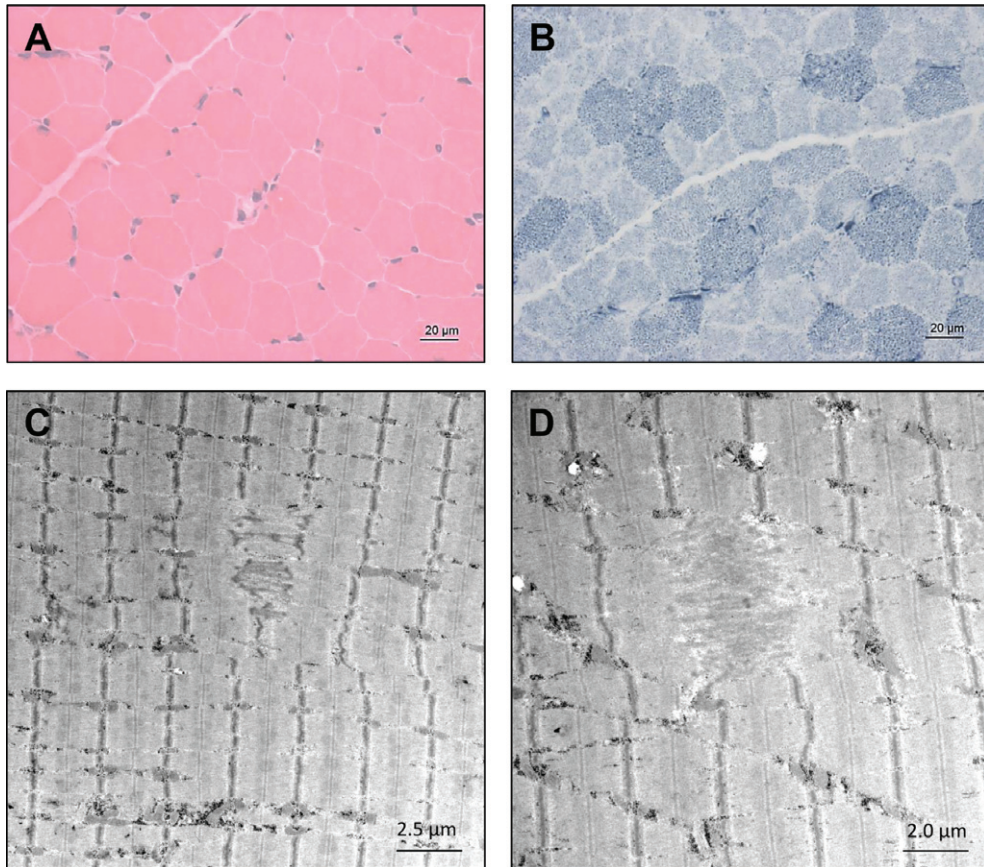


Fig. 2. Microscopic findings in NEFL-mutant muscle. Haematoxylin & Eosin (H&E) staining did not reveal striking myopathic changes (A) whereas NADH-TR in some muscle fibers revealed increased subsarcolemmal reactivity indicative for mitochondrial accumulations in addition to pale regions in sum indicating altered mitochondrial distribution (B, arrows). Electron microscopic studies revealed focal alterations of sarcomere pattern with streaming of Z-discs and incidental pronounced Z-disc disruption as minicore-like lesions and small cytoplasmic bodies (C and D, arrowhead).

biopsy (H&E staining shown in Fig. 2A) except the indication of altered mitochondrial distribution based on NADH-TR staining (Fig. 2B). However, ultra-structural studies utilizing electron microscopy unraveled focal alterations of sarcomere pattern with streaming of Z-discs and incidental pronounced Z-disc disruption as minicore-like lesions in addition to small cytoplasmic bodies (Fig. 2C & D). No larger autophagic vacuoles, or tubular aggregates were identified. Mitochondria presented with normal size and shape and no ultrastructural abnormalities of nuclei were found (data not shown).

Coherent anti-Stokes Raman scattering microscopy (CARS)

CARS offers the unique opportunity to investigate protein and lipid imbalances in an unbiased

manner by making use of a minimal amount of material and is thus a valuable analytical technique in the investigation of pathological features in biopsy material such as muscle biopsy specimens. Thus, we applied this label-free technique to obtain further unbiased insights into the muscle cell vulnerability underlying the pathogenic NEFL-variant. To locate spectroscopic features in the muscle biopsy samples (NEFL-patient 1 and controls), first the spectrum of the fibre background (areas in which no features) was defined, and a mean spectrum was calculated. The fibre background of NEFL-patient 1 (Fig. 3A, pBG) shows a lower signal intensity at 2921 cm^{-1} than at 2868 cm^{-1} . The signal at 2921 cm^{-1} is characteristic for proteinogenic content [43, 44]. The standard peak of ordered lipids [45] at 2889 cm^{-1} seems to be shifted to 2868 cm^{-1} . In contrast, in subsarcolemmal regions of NEFL-mutant muscle fibres, the intensity

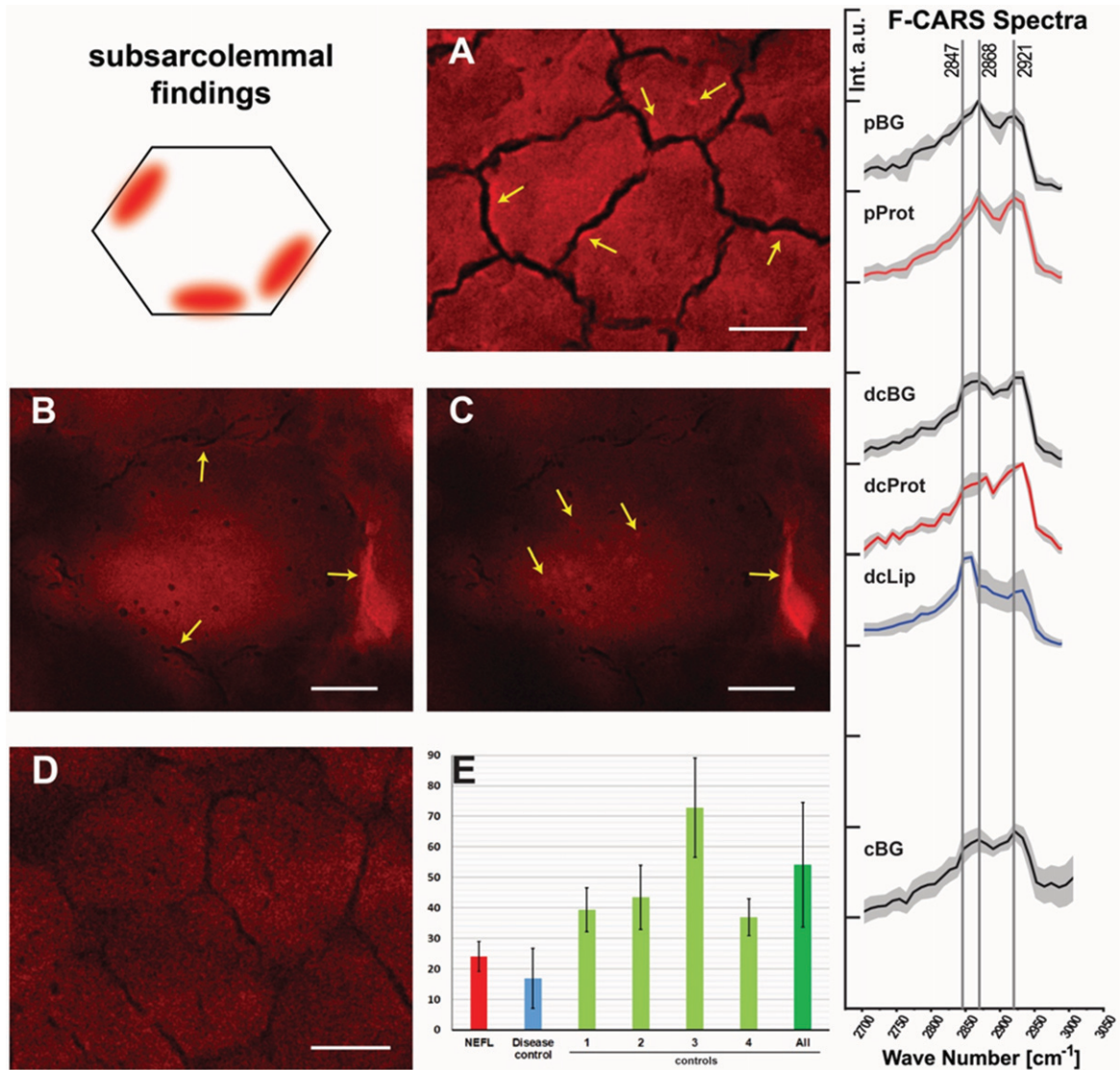


Fig. 3. Spectroscopic findings in *NEFL*-mutant muscle obtained by F-CARS measurements. Protein-containing regions in muscle fibres of *NEFL*-patient 1 at 2921 cm^{-1} (marked with arrows; scale bar $10\text{ }\mu\text{m}$) (**A**). Subsarcolemmal regions in muscle fibres of disease control present an increased signal at 2921 cm^{-1} (marked with arrows; scale bar $15\text{ }\mu\text{m}$) (**B**). Lipid features identified within and between muscle fibres of disease control with increased signal at 2847 cm^{-1} (marked with arrows; scale bar $15\text{ }\mu\text{m}$) (**C**). Muscle fibres of a representative healthy control (scale bar $10\text{ }\mu\text{m}$) (**D**). Comparison of the average muscle fibre calibres. *NEFL*-patient 1: $24.01\text{ }\mu\text{m} \pm 4.94\text{ }\mu\text{m}$ (721 fibres); disease control: $16.97\text{ }\mu\text{m} \pm 9.78\text{ }\mu\text{m}$ (782 fibres); controls: 1: $39.38\text{ }\mu\text{m} \pm 7.23\text{ }\mu\text{m}$ (318 fibres); 2: $43.48\text{ }\mu\text{m} \pm 10.49\text{ }\mu\text{m}$ (184 fibres); 3: $72.82\text{ }\mu\text{m} \pm 16.29\text{ }\mu\text{m}$ (436 fibres); 4: $19.62\text{ }\mu\text{m} \pm 3.62\text{ }\mu\text{m}$ (430 fibres); 5: $36.94\text{ }\mu\text{m} \pm 6.09\text{ }\mu\text{m}$ (89 fibres); all controls: $43.92\text{ }\mu\text{m} \pm 23.29\text{ }\mu\text{m}$ (1457 fibres) (**E**).

at 2921 cm^{-1} and 2868 cm^{-1} is comparable (Fig. 3A, pProt). For CARS A, a higher intensity for 2921 cm^{-1} based spectra can be observed in the subsarcolem-

mal regions compared to the fibre background. In the light of the above-mentioned aspects, we concluded based on these data that in *NEFL*-mutant muscle

demonstrates an increased protein content (mirrored by increased signal at 2921 cm^{-1}) is present in some regions of fibers.

Spectral analysis of the disease control (neurogenic muscular atrophy in the biopsy of an age-matched child) revealed differences in comparison to the NEFL-patient 1 (Fig. 3B & C). The fibre background (dcBG) shows a slightly higher intensity at 2921 cm^{-1} than at 2868 cm^{-1} . Thus, the spectrum is similar to that of the controls (Fig. 3D, cBG). Also, less pronounced subsarcolemmal spots with significantly increased signal at 2921 cm^{-1} were found in the disease control (Fig. 3, dcProt), but regions in and between fibres were also identified with high signal at 2847 cm^{-1} (Fig. 3C, dcLip). Especially disordered lipids show a strong signal at 2847 cm^{-1} . No lipid features were found, neither in controls nor in the NEFL-patient.

To investigate muscle fibre calibre, we measured the average of muscle cells in the biopsy derived from NEFL-patient 1 in comparison to a disease control (denervation atrophy) and normal controls: while the averaged muscle fibre calibre in the NEFL-patient 1's muscle biopsy is $24.01\text{ }\mu\text{m}\pm 4.94\text{ }\mu\text{m}$ (721 fibres), a calibre of $54.09\text{ }\mu\text{m}\pm 20.33\text{ }\mu\text{m}$ (1027 fibres) was detected in the normal controls and $16.97\text{ }\mu\text{m}\pm 9.78\text{ }\mu\text{m}$ (782 fibres) in the disease control (Fig. 3E). Thus, our CARS-based investigations also enabled to demonstrate smaller muscle fibre calibre in NEFL-patient 1, a microscopic finding which accords with the assumption of neuropathy-related denervation.

Proteomic profiling of NEFL-mutant muscle derived from patient 1

To identify the proteins (reflecting molecular processes) underlying the pathogenic NEFL variant in skeletal muscle, we performed label-free untargeted proteomic profiling on quadriceps muscles derived from patient 1 in comparison to three healthy age- and gender-matched controls (Fig. 4A). By measuring 5777 unique peptides (Fig. 4B), we identified 58 proteins with an increased abundance of more than 1.3-fold whereas 60 proteins were identified with a decrease of a minimum of 0.7-fold (Fig. 4C & Table 2). These 118 altered proteins were quantified based on at least two unique peptides and significantly dysregulated with a $p\text{-ANOVA} \leq 0.05$ (Table 2). All functional information about these dysregulated proteins listed in Table 1 was extracted from uniprot (www.uniprot.org, accessed on 10th of March 2023).

We performed GO term analysis focussing on the up- and down-regulated proteins separately (Fig. 4D): within the group of upregulated proteins, the most altered biological processes include organization of the extracellular matrix including collagen fibril organization (indicative for fibrotic processes), activity of complex I of mitochondrial respiratory chain and metabolic processes of reactive oxygen species and carbohydrates, tricarboxylic acid cycle, axogenesis including axon extension involved in axon guidance, chaperone-mediated protein folding and muscle contraction (Fig. 4B). Molecular functions affected by increased proteins contain oxidoreductase activity including NADH dehydrogenase activity and electron carrier activity, extracellular matrix structural constituent and matrix binding, double-stranded RNA binding, activities of superoxide dismutase and thioester hydrolase, binding of proteins to chaperones (to warrant proper folding) and muscle alpha-actinin protein binding (Fig. 4D). In accordance with affected biological processes and molecular functions, affected cellular compartments include the extracellular matrix, mitochondria, lumen of Golgi apparatus and lysosomes, peroxisomes, nuclear chromatin, sarcolemma including membrane rafts, actin cytoskeleton and the myelin sheath (Fig. 4D). A GO-term-based pathway analysis of down regulated proteins revealed that a significant proportion of these proteins affect different biological processes including glycolysis, tricarboxylic acid cycle, mitochondrial acetyl-CoA biosynthetic processes, creatine metabolic processes, muscle organ development and functions such as muscle contraction and myofibril assembly. Molecular functions affected by decreased protein abundances contain structural constituent of muscle and cytoskeleton (including binding of cytoskeletal proteins such as titin and tropomyosin), ion channel binding as well as activities of structural proteins and pyruvate dehydrogenases (Fig. 4D). In line with the affected biological processes and molecular functions decreased proteins impact on myelin sheath, extracellular matrix, myonuclei, mitochondria and the sarcomeric system (Z-disc, I and M bands, actin and thin filaments) (Fig. 4D).

DISCUSSION

Pathogenic variants in *NEFL* have been frequently linked to manifestation of different subtypes of CMT neuropathy, CMT1F and CMT2E and an intermediate

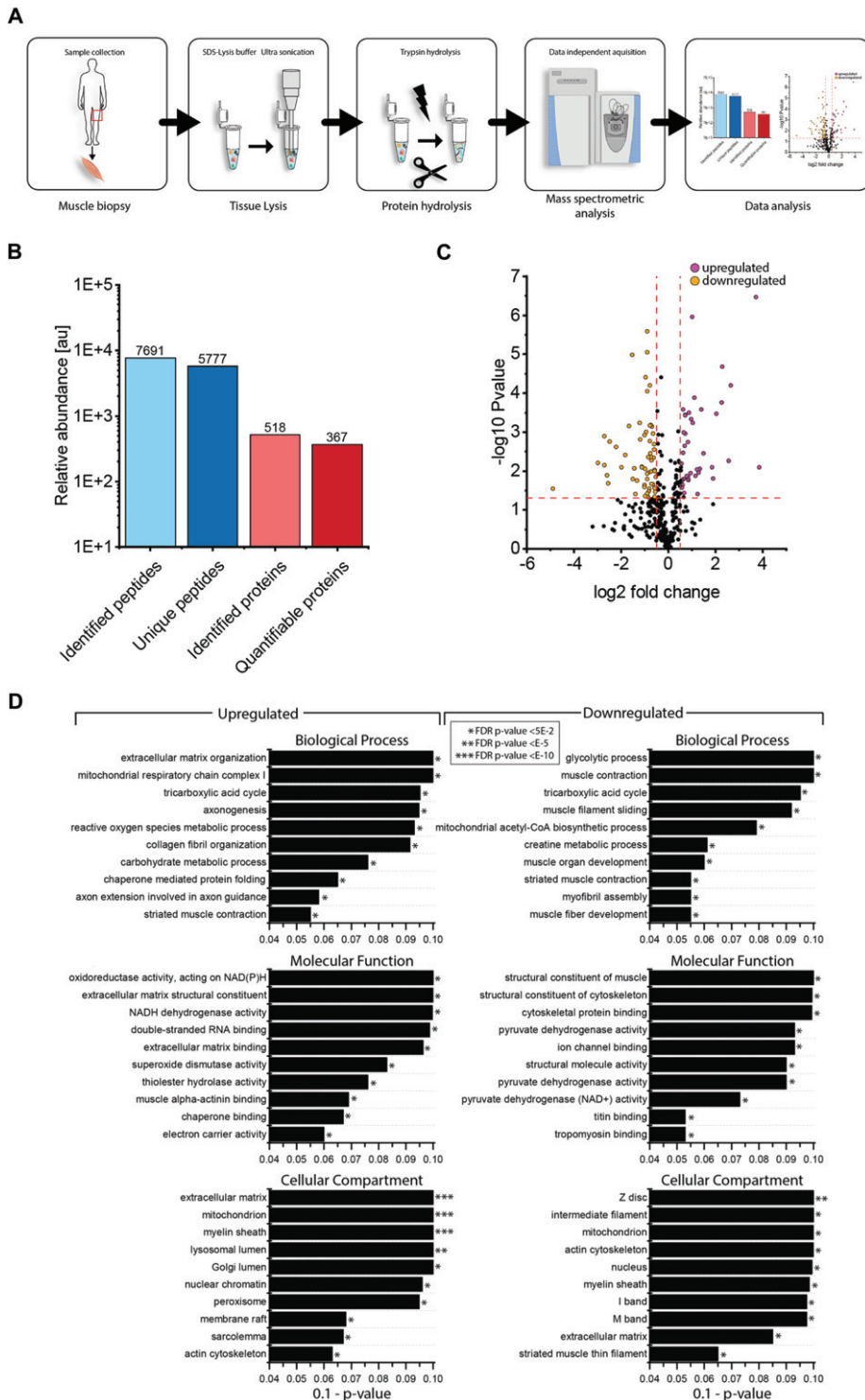


Fig. 4. Proteomic profiling of *NEFL*-mutant muscle. (A) Schematic representation of our workflow applied to decipher the proteomic changes in *NEFL*-mutant muscle. (B) Statistics of our proteomic findings. (C) Volcano-plot indicating the statistically significant dysregulated proteins. Increased proteins are highlighted as purple dots whereas decreased proteins are depicted as orange dots. (D) Results of in silico based (GO-term) analysis of the proteomic signature of *NEFL*-mutant muscle indicating biological processes, molecular functions and subcellular structures affected by the dysregulated proteins, respectively.

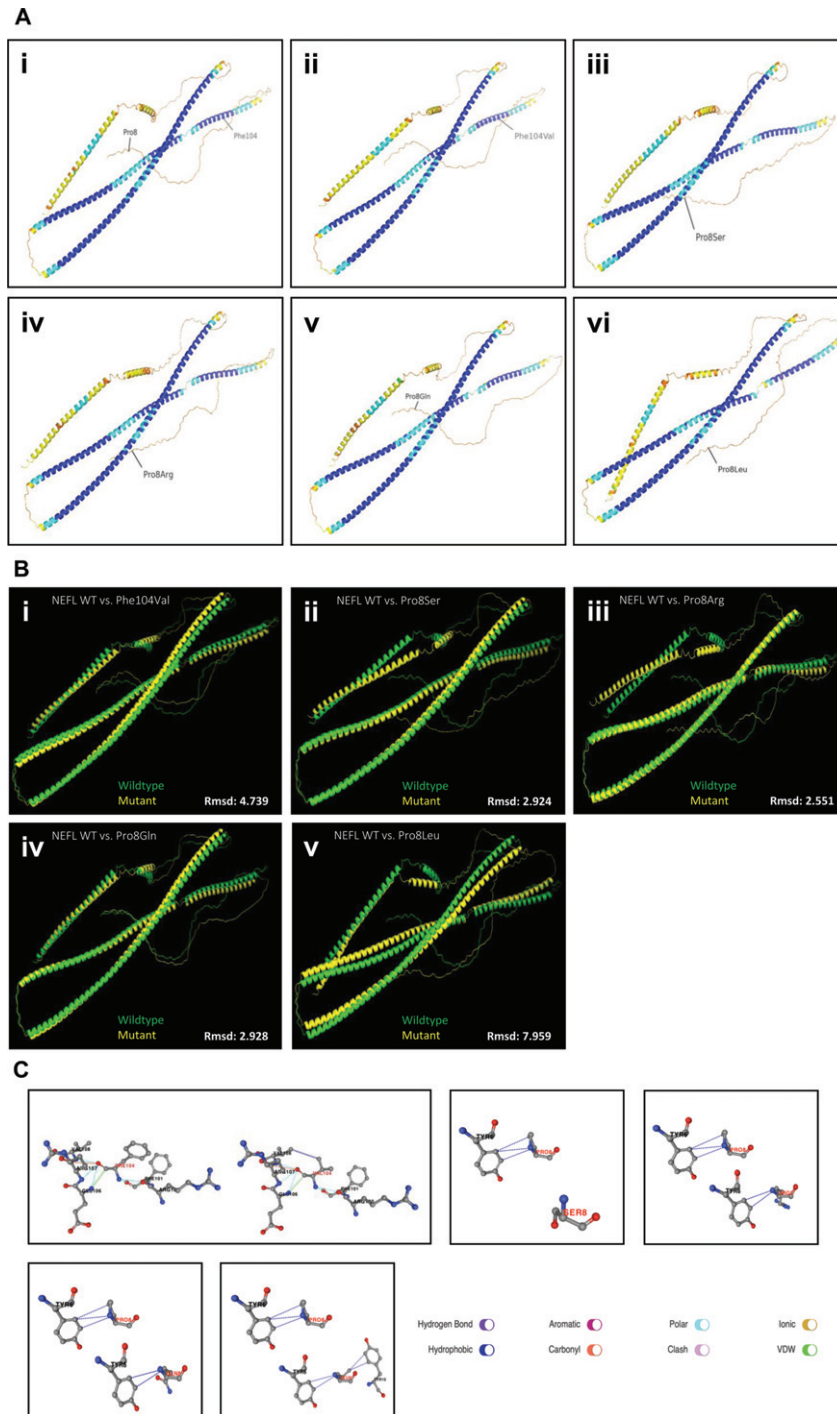


Fig. 5. *In silico* studies on amino acid substitutions affecting NEFL. (A) ColabFold predictions of three-dimensional protein structure of (i) Wild-type (WT) NEFL (ii) Phe104Val (iii) Pro8Ser (iv) Pro8Arg (v) Pro8Gln (vi) Pro8Leu. Residues are colour-coded on a spectrum of dark blue to red based on pLDDT score, with blue representing high pLDDT and red representing low pLDDT. WT NEFL pLDDT: 72.2, Phe104Val pLDDT: 72.2, Pro8Ser pLDDT: 72.4, Pro8Arg pLDDT: 72.2, Pro8Gln pLDDT: 71.8, Pro8Leu pLDDT: 72. (B) Root-mean-square deviation (Rmsd) scores calculated from superimpositions of each NEFL protein variant with the WT NEFL protein structure. Superimpositions were performed in PyMOL. (C) PremPS predictions of differences in hydrophobic interactions between mutated residues and adjacent residues in NEFL variants compared to WT NEFL.

Table 2
List of statistically significant dysregulated proteins including number of unique peptides identified for each protein

Accession #	Unique peptides	Description	Ratio	p-value
O60938	3	Keratocan (KERA_HUMAN)	14.52	0.008
Q06828	5	Fibromodulin (FMOD_HUMAN)	13.26	0.000
P14854	2	Cytochrome c oxidase subunit 6B1 (CX6B1_HUMAN)	6.32	0.000
P02452	7	Collagen alpha-1(I) chain (CO1A1_HUMAN)	5.91	0.006
Q8WZ42	1271	Titin (TITIN_HUMAN)	4.95	0.000
P21810	2	Biglycan (PGS1_HUMAN)	4.83	0.000
P51888	10	Prolargin (PRELP_HUMAN)	4.15	0.000
P08123	9	Collagen alpha-2(I) chain (CO1A2_HUMAN)	3.73	0.016
Q7Z5Q5	2	DNA polymerase nu (DPOLN_HUMAN)	3.64	0.008
P60903	2	Protein S100-A10 (S10AA_HUMAN)	2.83	0.004
P07942	2	Laminin subunit beta-1 (LAMB1_HUMAN)	2.64	0.000
P20774	11	Mimecan (MIME_HUMAN)	2.54	0.009
P08670	23	Vimentin (VIME_HUMAN)	2.46	0.011
P07195	7	L-lactate dehydrogenase B chain (LDHB_HUMAN)	2.37	0.040
P07585	16	Decorin (PGS2_HUMAN)	2.34	0.009
Q15582	4	Transforming growth factor-beta-induced protein ig-h3 (BGH3_HUMAN)	2.25	0.013
P48735	14	Isocitrate dehydrogenase [NADP], mitochondrial (IDHP_HUMAN)	2.18	0.000
P54289	2	Voltage-dependent calcium channel subunit alpha-2/delta-1 (CA2D1_HUMAN)	2.07	0.001
P62937	8	Peptidyl-prolyl cis-trans isomerase A (PIIA_HUMAN)	2.03	0.000
P49753	5	Acyl-coenzyme A thioesterase 2, mitochondrial (ACOT2_HUMAN)	1.96	0.000
Q09666	4	Neuroblast differentiation-associated protein AHNAK (AHNK_HUMAN)	1.95	0.012
P09429	2	High mobility group protein B1 (HMGB1_HUMAN)	1.85	0.000
P35579	2	Myosin-9 (MYH9_HUMAN)	1.82	0.017
P10809	4	60 kDa heat shock protein, mitochondrial (CH60_HUMAN)	1.80	0.002
P49821	4	NADH dehydrogenase [ubiquinone] flavoprotein 1, mitochondrial (NDUV1_HUMAN)	1.79	0.016
P05091	3	Aldehyde dehydrogenase, mitochondrial (ALDH2_HUMAN)	1.79	0.015
P30048	6	Thioredoxin-dependent peroxide reductase, mitochondrial (PRDX3_HUMAN)	1.75	0.013
P00505	17	Aspartate aminotransferase, mitochondrial (AATM_HUMAN)	1.66	0.001
P10412	7	Histone H1.4 (H14_HUMAN)	1.65	0.000
P08758	9	Annexin A5 (ANXA5_HUMAN)	1.65	0.000
Q04760	3	Lactoylglutathione lyase (LGUL_HUMAN)	1.63	0.002
P02545	18	Prelamin-A/C (LMNA_HUMAN)	1.61	0.037
O75306	2	NADH dehydrogenase [ubiquinone] iron-sulfur protein 2, mitochondrial (NDUS2_HUMAN)	1.58	0.001
P49411	4	Elongation factor Tu, mitochondrial (EFTU_HUMAN)	1.57	0.048
O14958	10	Calsequestrin-2 (CASQ2_HUMAN)	1.57	0.017
P61981	9	14-3-3 protein gamma (1433G_HUMAN)	1.56	0.000
Q16795	8	NADH dehydrogenase [ubiquinone] 1 alpha subcomplex subunit 9, mitochondrial (NDUA9_HUMAN)	1.55	0.004
Q6YN16	2	Hydroxysteroid dehydrogenase-like protein 2 (HSDL2_HUMAN)	1.53	0.023
Q9UMS6	6	Synaptopodin-2 (SYNP2_HUMAN)	1.51	0.017
P00441	3	Superoxide dismutase [Cu-Zn] (SODC_HUMAN)	1.51	0.027
O43181	2	NADH dehydrogenase [ubiquinone] iron-sulfur protein 4, mitochondrial (NDUS4_HUMAN)	1.49	0.019
P07437	3	Tubulin beta chain (TBB5_HUMAN)	1.48	0.007
P16104	2	Histone H2AX (H2AX_HUMAN)	1.47	0.008
Q16777	2	Histone H2A type 2-C (H2A2C_HUMAN)	1.47	0.010
P04179	9	Superoxide dismutase [Mn], mitochondrial (SODM_HUMAN)	1.44	0.018
P12110	12	Collagen alpha-2(VI) chain (CO6A2_HUMAN)	1.44	0.038
P42765	9	3-ketoacyl-CoA thiolase, mitochondrial (THIM_HUMAN)	1.41	0.025
Q08623	2	Pseudouridine-5'-phosphatase (HDHD1_HUMAN)	1.41	0.010
P07954	10	Fumarate hydratase, mitochondrial (FUMH_HUMAN)	1.39	0.010

(Continued)

Table 2
(Continued)

Accession #	Unique peptides	Description	Ratio	p-value
P31946	2	14-3-3 protein beta/alpha (1433B_HUMAN)	1.39	0.006
P30042	6	ES1 protein homolog, mitochondrial (ES1_HUMAN)	1.38	0.022
P53597	2	Succinate-CoA ligase [ADP/GDP-forming] subunit alpha, mitochondrial (SUCA_HUMAN)	1.37	0.006
P28331	6	NADH-ubiquinone oxidoreductase 75 kDa subunit, mitochondrial (NDUS1_HUMAN)	1.36	0.001
Q00610	2	Clathrin heavy chain 1 (CLH1_HUMAN)	1.35	0.047
P06396	11	Gelsolin (GELS_HUMAN)	1.34	0.042
Q9NZU5	6	LIM and cysteine-rich domains protein 1 (LMCD1_HUMAN)	1.32	0.037
P61604	2	10 kDa heat shock protein, mitochondrial (CH10_HUMAN)	1.30	0.020
Q16698	3	2,4-dienoyl-CoA reductase, mitochondrial (DECR_HUMAN)	1.30	0.009
Q8NB12	8	Histone-lysine N-methyltransferase SMYD1 (SMYD1_HUMAN)	0.70	0.014
P10916	41	Myosin regulatory light chain 2, ventricular/cardiac muscle isoform (MLRV_HUMAN)	0.69	0.035
P09669	3	Cytochrome c oxidase subunit 6 C (COX6C_HUMAN)	0.68	0.028
P52179	63	Myomesin-1 (MYOM1_HUMAN)	0.68	0.009
Q14353	3	Guanidinoacetate N-methyltransferase (GAMT_HUMAN)	0.68	0.046
P13805	20	Troponin T, slow skeletal muscle (TNNT1_HUMAN)	0.67	0.010
O00499	13	Myc box-dependent-interacting protein 1 (BIN1_HUMAN)	0.67	0.002
P13929	39	Beta-enolase (ENOB_HUMAN)	0.66	0.003
P20929	272	Nebulin (NEBU_HUMAN)	0.65	0.005
P07237	2	Protein disulfide-isomerase (PDIA1_HUMAN)	0.65	0.001
P22061	4	Protein-L-isoaspartate(D-aspartate) O-methyltransferase (PIMT_HUMAN)	0.64	0.022
P04080	2	Cystatin-B (CYTB_HUMAN)	0.64	0.052
P11177	8	Pyruvate dehydrogenase E1 component subunit beta, mitochondrial (ODPB_HUMAN)	0.63	0.001
P30086	10	Phosphatidylethanolamine-binding protein 1 (PEBP1_HUMAN)	0.62	0.022
Q9UHQ9	7	NADH-cytochrome b5 reductase 1 (NB5R1_HUMAN)	0.61	0.005
P11142	15	Heat shock cognate 71 kDa protein (HSP7C_HUMAN)	0.61	0.011
Q53GG5	11	PDZ and LIM domain protein 3 (PDLI3_HUMAN)	0.61	0.001
Q9NP98	17	Myozenin-1 (MYOZ1_HUMAN)	0.60	0.004
P15259	14	Phosphoglycerate mutase 2 (PGAM2_HUMAN)	0.60	0.004
Q9H987	2	Synaptopodin 2-like protein (SYP2L_HUMAN)	0.58	0.002
P14927	2	Cytochrome b-c1 complex subunit 7 (QCR7_HUMAN)	0.58	0.001
P31415	27	Calsequestrin-1 (CASQ1_HUMAN)	0.58	0.000
Q9BWH2	2	FUN14 domain-containing protein 2 (FUND2_HUMAN)	0.57	0.029
P43155	4	Carnitine O-acetyltransferase (CACP_HUMAN)	0.57	0.034
Q13642	11	Four and a half LIM domains protein 1 (FHL1_HUMAN)	0.56	0.011
Q9NZQ9	6	Tropomodulin-4 (TMOD4_HUMAN)	0.56	0.005
P46976	4	Glycogenin-1 (GLYG_HUMAN)	0.56	0.048
P16989	5	Y-box-binding protein 3 (YBOX3_HUMAN)	0.54	0.045
P21796	12	Voltage-dependent anion-selective channel protein 1 (VDAC1_HUMAN)	0.54	0.000
P00558	26	Phosphoglycerate kinase 1 (PGK1_HUMAN)	0.54	0.039
P36871	29	Phosphoglucomutase-1 (PGM1_HUMAN)	0.54	0.012
Q9H6F2	3	Trimeric intracellular cation channel type A (TM38A_HUMAN)	0.54	0.016
P08559	8	Pyruvate dehydrogenase E1 component subunit alpha, somatic form, mitochondrial (ODPA_HUMAN)	0.54	0.000
P17540	11	Creatine kinase S-type, mitochondrial (KCRS_HUMAN)	0.54	0.000
Q99497	8	Protein/nucleic acid deglycase DJ-1 (PARK7_HUMAN)	0.52	0.001
P63241	2	Eukaryotic translation initiation factor 5A-1 (IF5A1_HUMAN)	0.51	0.000
Q9Y235	5	C->U-editing enzyme APOBEC-2 (ABEC2_HUMAN)	0.51	0.045
P07108	3	Acyl-CoA-binding protein (ACBP_HUMAN)	0.51	0.009
P09382	3	Galectin-1 (LEG1_HUMAN)	0.50	0.023
Q9UHG3	2	Prenylcysteine oxidase 1 (PCYOX_HUMAN)	0.50	0.026

(Continued)

Table 2
(Continued)

Accession #	Unique peptides	Description	Ratio	p-value
P0DP23	3	Calmodulin-1 (CALM1_HUMAN)	0.50	0.001
Q14315	94	Filamin-C (FLNC_HUMAN)	0.46	0.008
Q9NX63	2	MICOS complex subunit MIC19 (MIC19_HUMAN)	0.46	0.008
Q9NRX4	6	14 kDa phosphohistidine phosphatase (PHP14_HUMAN)	0.44	0.002
P07451	22	Carbonic anhydrase 3 (CAH3_HUMAN)	0.44	0.001
Q9GZV1	5	Ankyrin repeat domain-containing protein 2 (ANKR2_HUMAN)	0.40	0.018
P09972	2	Fructose-bisphosphate aldolase C (ALDOC_HUMAN)	0.38	0.040
P14618	41	Pyruvate kinase PKM (KPYM_HUMAN)	0.37	0.009
P08779	2	Keratin, type I cytoskeletal 16 (K1C16_HUMAN)	0.35	0.016
O14880	2	Microsomal glutathione S-transferase 3 (MGST3_HUMAN)	0.35	0.000
Q99798	23	Aconitate hydratase, mitochondrial (ACON_HUMAN)	0.31	0.001
P02533	2	Keratin, type I cytoskeletal 14 (K1C14_HUMAN)	0.28	0.004
P13645	21	Keratin, type I cytoskeletal 10 (K1C10_HUMAN)	0.25	0.008
P35908	8	Keratin, type II cytoskeletal 2 epidermal (K22E_HUMAN)	0.22	0.002
Q9UHP9	2	Small muscular protein (SMPX_HUMAN)	0.18	0.002
Q9BXS1	2	Isopentenyl-diphosphate delta-isomerase 2 (IDI2_HUMAN)	0.17	0.021
P23297	4	Protein S100-A1 (S10A1_HUMAN)	0.17	0.013
P13647	2	Keratin, type II cytoskeletal 5 (K2C5_HUMAN)	0.15	0.007
P04264	24	Keratin, type II cytoskeletal 1 (K2C1_HUMAN)	0.15	0.001
P35527	18	Keratin, type I cytoskeletal 9 (K1C9_HUMAN)	0.13	0.006
Q86YZ3	5	Hornerin (HORN_HUMAN)	0.03	0.029

form [46]. Most pathogenic *NEFL* variants are dominant missense variants functioning through a gain-of-function mechanism in which amino acid substitutions within the corresponding protein disrupt neurofilament assembly and thus impact organelle transport within cells of the peripheral nervous system. All reported homozygous nonsense variants follow a recessive mode of inheritance [13–15]. Besides *NEFL* serves as a biomarker in cerebrospinal fluid of neurodegenerative diseases such as Amyotrophic Lateral Sclerosis and 5q-related spinal muscular atrophy. Furthermore, a transgenic mouse model of a mutant neurofilament light chain p.(Leu394Pro) shows loss of ventral horn motor neurons and denervation atrophy of the skeletal muscle suggesting that *NEFL* may also be a candidate gene for motor neuron diseases [47]. These combined findings suggest a profound role of the protein in maintenance of the nervous system. However, studies aiming to decipher molecular processes associated with porcine intrauterine muscle cell development revealed that altered *Nefl* expression is associated with the process of primary to secondary myofibers formation [23] in turn suggesting a functional role of the neurofilament light chain protein in muscle. Of note, based on cases presenting with pathogenic variants in *NEFL* associated with the manifestation of primary myopathic features, there is growing evidence for a functional role of this intermediate

filament also in skeletal muscle: one family with 4 affected members (mother and her three sons all carrying the c.1261C>T variant) presented with different pathomorphological findings in the muscle biopsy: in addition to neuropathic features (including type II fiber predominance, grouped fiber atrophy, and small angular fibers), pathomorphological findings such as Nemaline bodies indicative for a primary vulnerability of muscle cells (myopathy) were identified [17]. The NCV and muscle biopsy findings (including determination of muscle fibre calibre by CARS) in our *NEFL*-patient 1 were compatible with neurogenic process. However, neuropathic changes occasionally can be seen in a chronic myopathic process with *GFPT1*- and *BICD2*-related neuropathologies being prominent examples [48, 49]. In a previous study, we reported on a family presenting with the c.1186G>A; p.(Glu396Lys) variant not only associated with mixed axonal and demyelinating neuropathy but also with considerably elevated CK levels in all affected adults of the family as well as pronounced myopathic changes in skeletal muscle biopsies (increased number of internalized myonuclei, myophagic reaction indicating muscle fibre break down) pointing towards an accompanying muscle involvement as a primary target [22]. These data already suggest a clinical variability associated with pathogenic *NEFL* variants and indeed recently a novel *NEFL* variant (c.1319C>T) was linked to the manifestation of a

mild form of CMT2E associated with liability to pressure palsy (HNPP) [50]. Moreover, another recent study described cohort of *NEFL* patients presenting with an intermediate form of neuropathy complicated a range of symptoms including cardiac conduction abnormalities [51].

Important to note, our patient 1 presented with muscle cramps and muscular stiffness as first clinical symptoms, indicative – in combination with mildly elevated CK levels – for primary muscular involvement in terms of myopathy impacting on diagnostic work-up (including microscopic studies on muscle biopsy). Hence, here, we link the c.310T>G; p.(Phe104Val) variant to the manifestation of a mild neuropathy associated with muscle symptoms defined by cramps, mildly elevated CK level and focal myofibrillar alterations with minicore-like disintegration of sarcomeric structures. In this context it is important to note that different degenerative changes in Z-disc integrity were already linked to neuropathies defined by axonal pathology with decrease of neurofilaments and microtubules in myelinated and unmyelinated nerves [52]. Thus, that ultrastructural pathology of sarcomeres in our patient may result from denervation, as already hypothesized by Agrawal and colleagues describing a family with a primary neuropathic phenotype in the context of the extremely low expression of *NEFL* in skeletal musculature [17]. However, further mycological studies for instance on a suitable animal model are crucial to draw final conclusions.

CARS microscopic studies on the muscle biopsy specimen derived from our patient 1 in comparison to non-disease controls as well as a disease control (muscle denervation) revealed presence of subsarcolemmal protein enrichment and investigation of the proteomic signature unravelled dysregulation of proteins according with the ultra-structural findings: a variety of cytoskeletal proteins were dysregulated including FLNc as a protein for which pathogenic variants have been linked to a muscle disease called myofibrillar myopathy, which is characterized by disintegration of sarcomeric structures. Increased expression of chaperones (needed for protein folding) was also identified in patient 1's quadriceps muscle. Further biochemical studies – such as proteomics - on denervated muscle are crucial to elucidate the impact of FLNc (and other structural proteins) as well as of chaperones on disintegration of sarcomeric structures resulting from perturbed neuromuscular transmission.

Regarding the broad clinical manifestation of pathogenic *NEFL* variants, it is important to note that recently, also central nervous system (CNS) affection including abnormal MRI findings, dementia and dysarthria have been described [53–55]. Already Kim and colleagues postulated that *NEFL* plays also a role in the CNS and supported this assumption by the finding of multiple inclusions in cell bodies and proximal axons of the spinal cord, cerebellum, pons, and cerebral cortex in *Nefl*-mouse model (heterozygous p.(Asn98Ser) variant) [53]. Moreover, in *NEFL*-patients carrying the p.(Glu90Lys) and p.(Asn98Ser) amino acid substitutions, intellectual impairment was present [16]. Thus, we consider the intellectual disability present in our patient 1 also as a part of CNS involvement. However, his cranial MRI at the age of two years was normal.

One might speculate that the pathogenicity of respective amino acid substitutions or expression of modifying factors contribute to the phenotypical manifestation and thus broad neurological/neuromuscular spectrum associated with pathogenic variants in *NEFL*. Indeed, further functional studies on patient derived material are needed to prove this assumption. Another explanation for clinical (intra-familial) variability is provided by our familiar cases presented in this study: while patient 2 presents a neuropathy-phenotype (NCV at the age of 16 years revealed demyelinating pattern) with slow progressive muscular weakness, mild peripheral ataxia and reduced walking distance and pes cavus, her father had a non-progressive pes cavus with normal muscle strength, absent ATR and minimal neuropathic pattern as observed by the results of NCV measurement. Of note, while molecular genetic studies on DNA derived from the daughter clearly revealed the c.22C>T p.(Pro8Ser) variant, the same variant was detected only in 15% of reads indicative for mosaicism. Interestingly, three other amino acid substitutions affecting the same position (p.(Pro8Arg), p.(Pro8Gln) & p.(Pro8Leu)) have been described before [38]. A clinical comparison revealed that these variants are associated with both, a more (p.(Pro8Leu) & p.(Pro8Gln)) as well as a less severe (p.(Pro8Arg)) phenotype than observed in our patient. Intra-familial variability has been described in the context of clinical manifestation of pathogenic *NEFL* variants and should thus carefully be taken into consideration in the delineation of the attempts of genotype-phenotype correlations. Along this line, a muscular phenotype segregating in a family with four affected members included different grades of

severity of clinical manifestation [17]. One might speculate that the presence of modifiers may explain the varying manifestation. However, comprehensive molecular studies on intrafamilial biosamples would be needed to systematically address this assumption. Nevertheless, it has been postulated that disease is not only caused by impairment of domain-specific functions of NEFL or neurofilaments but rather by general perturbations in protein folding or stability leading to pathological changes in neurofilament subunit stoichiometry, or to protein aggregation and cellular stress [2, 53]. Along this line, more than 170 patients with pathogenic *NEFL* variants have been reported with broad age-range of the onset of the symptoms [2, 16] and it was postulated that pathogenic variants affecting the head domain lead to an earlier manifestation of the phenotype. Our *in silico* based modelling of missense variants affecting the amino acid proline at position 8 revealed a varying pathogenic impact of the respective amino acid substitutions either resulting in stabilization or destabilization of the protein. According to the clinical data available for our patient and in the literature one might speculate that stabilizing variants such as p.(Pro8Leu) and p.(Pro8Ser) are associated with an earlier disease manifestation. Of course, the current number of cases presenting with pathogenic variants affecting proline at position 8 of NEFL is too small to draw final conclusions and the possibility of other factors such as genetic modifiers also need to be considered. However, our combined clinical and molecular genetic findings support this assumption by introducing the p.(Pro8Ser) amino acid substitution as a novel *NEFL* variant extending the current molecular genetic landscape for this gene with an associated early clinical manifestation.

CONCLUSIONS

Based on our combined data, we expand the current molecular genetic landscape of NEFL-associated neuropathies by linking the c.22C>T; p.(Pro8Ser) variant to the manifestation of neuropathic features and along this line introduce the same variant in mosaicism in the mildly affected patient's father. Hence, this is the first report of a pathogenic somatic NEFL variant. Given that different amino acid substitutions for position 8 were associated with diverging neuropathic manifestations, *in silico* modelling of these variants was performed and results suggest a link between protein misfolding and age of onset.

Moreover, our report on a boy with a NEFL variant known to cause neuropathy but also suffering from muscular symptoms (supported by microscopic and biochemical data) supports the concept that NEFL variants may have different clinical manifestations along the neuromuscular axis. Although, our data obtained in the latter patient imply additional muscle cell vulnerability upon the expression of mutant NEFL, the effect of denervation on morphological and biochemical integrity must be taken into consideration. Hence, further studies – for instance on human muscle organoids expressing mutant NEFL – would be needed to decipher the exact impact of the intermediate filament protein for proper muscle cell function.

AUTHOR CONTRIBUTIONS

AR, HK and ADM conceptualized and designed the study, drafted the first version of the manuscript, interpreted results and are principally responsible for the final content. USS and TR reviewed and revised the manuscript for important intellectual content. JW performed the electron microscopic studies. AH performed the proteomic studies. AC, AA, AL and AS analyzed data and interpreted results. *In silico* modelling was performed by HL and CC. All authors contributed to the final manuscript and agreed to be accountable for all aspects of the work.

ACKNOWLEDGMENTS

The authors are grateful to the families for cooperation and for the permission to publish the data. Four authors of this publication are members of the European Reference Network for Neuromuscular Diseases – Project ID N° 870177.

FUNDING

AR received funding from The French Muscular Dystrophy Association (AFM-Téléthon) (grant 21644). AR and USS also acknowledge funding in the framework of the NME-GPS project by the European Regional Development Fund (ERDF).

HL receives support from the Canadian Institutes of Health Research (CIHR) for Foundation Grant FDN-167281 (Precision Health for Neuromuscular Diseases), Transnational Team Grant ERT-174211 (ProDGNE) and Network Grant OR2-189333 (NMD4C), from the Canada Foundation for

Innovation (CFI-JELF 38412), the Canada Research Chairs program (Canada Research Chair in Neuromuscular Genomics and Health, 950-232279), the European Commission (Grant # 101080249) and the Canada Research Coordinating Committee New Frontiers in Research Fund (NFRFG-2022-00033) for SIMPATHIC, and from the Government of Canada Canada First Research Excellence Fund (CFREF) for the Brain-Heart Interconnectome (CFREF-2022-00007).

CONFLICTS OF INTEREST

The authors have no conflict of interest to report.

DATA AVAILABILITY STATEMENT

The data that support the findings of this study are available from the corresponding author upon request.

REFERENCES

- [1] Zhu Q, Couillard-Després S, Julien JP. Delayed Maturation of Regenerating Myelinated Axons in Mice Lacking Neurofilaments. *Exp Neurol* 1997;148:299–316. <https://doi.org/10.1006/exnr.1997.6654>.
- [2] Stone EJ, Kolb SJ, Brown A. A review and analysis of the clinical literature on Charcot–Marie–Tooth disease caused by mutations in neurofilament protein L. *Cytoskeleton* 2021;78:97–110. <https://doi.org/10.1002/cm.21676>
- [3] Prokop A. Cytoskeletal organization of axons in vertebrates and invertebrates. *J Cell Biol* 2020;219(7):e201912081. <https://doi.org/10.1083/JCB.201912081>
- [4] Liu YL, Guo YS, Xu L, Wu SY, Wu DX, Yang C, et al. Alternation of neurofilaments in immune-mediated injury of spinal cord motor neurons. *Spinal Cord* 2009;47:166–70. <https://doi.org/10.1038/sc.2008.90>
- [5] Hawley ZCE, Campos-Melo D, Strong MJ. MiR-105 and miR-9 regulate the mRNA stability of neuronal intermediate filaments. Implications for the pathogenesis of amyotrophic lateral sclerosis (ALS). *Brain Res* 2019;1706:93–100. <https://doi.org/10.1016/j.brainres.2018.10.032>
- [6] Perrot R, Eyer J. Neuronal intermediate filaments and neurodegenerative disorders. *Brain Res Bull* 2009;80:282–95. <https://doi.org/10.1016/j.brainresbull.2009.06.004>
- [7] Oeckl P, Weydt P, Thal DR, Weishaupt JH, Ludolph AC, Otto M. Proteomics in cerebrospinal fluid and spinal cord suggests UCHL1, MAP2 and GPNMB as biomarkers and underpins importance of transcriptional pathways in amyotrophic lateral sclerosis. *Acta Neuropathol* 2020;139:119–34. <https://doi.org/10.1007/s00401-019-02093-x>
- [8] Swindell WR, Kruse CPS, List EO, Berryman DE, Kopchick JJ. ALS blood expression profiling identifies new biomarkers, patient subgroups, and evidence for neutrophilia and hypoxia. *J Transl Med* 2019;17:170. <https://doi.org/10.1186/s12967-019-1909-0>
- [9] Olsson B, Portelius E, Cullen NC, Sandelius Å, Zetterberg H, Andreasson U, et al. Association of Cerebrospinal Fluid Neurofilament Light Protein Levels with Cognition in Patients with Dementia, Motor Neuron Disease, and Movement Disorders. *JAMA Neurol* 2019;76:318–25. <https://doi.org/10.1001/jamaneurol.2018.3746>
- [10] Ashton NJ, Janelidze S, Al Khleifat A, Leuzy A, van der Ende EL, Karikari TK, et al. A multicentre validation study of the diagnostic value of plasma neurofilament light. *Nat Commun* 2021;12:41. <https://doi.org/10.1038/s41467-021-23620-z>
- [11] Herrmann H, Aebi U. Intermediate filaments: Structure and assembly. *Cold Spring Harb Perspect Biol* 2016;8(11):a018242. <https://doi.org/10.1101/cshperspect.a018242>
- [12] Sainio MT, Ylikallio E, Mäenpää L, Lahtela J, Mattila P, Auranen M, et al. Absence of NEFL in patient-specific neurons in early-onset Charcot-Marie-Tooth neuropathy. *Neurol Genet* 2018;4(3):e244. <https://doi.org/10.1212/NXG.0000000000000244>
- [13] Yum SW, Zhang J, Mo K, Li J, Scherer SS. A novel recessive NEFL mutation causes a severe, early-onset axonal neuropathy. *Ann Neurol* 2009;66:759–70. <https://doi.org/10.1002/ana.21728>
- [14] Abe A, Numakura C, Saito K, Koide H, Oka N, Honma A, et al. Neurofilament light chain polypeptide gene mutations in Charcot-Marie-Tooth disease: Nonsense mutation probably causes a recessive phenotype. *J Hum Genet* 2009;54:94–7. <https://doi.org/10.1038/jhg.2008.13>
- [15] Fu J, Yuan Y. A novel homozygous nonsense mutation in NEFL causes autosomal recessive Charcot–Marie–Tooth disease. *Neuromuscul Disord* 2018;28:44–7. <https://doi.org/10.1016/j.nmd.2017.09.018>
- [16] Horga A, Laurà M, Jaunmuktane Z, Jerath NU, Gonzalez MA, Polke JM, et al. Genetic and clinical characteristics of NEFL-Related Charcot-Marie-Tooth disease. *J Neurol Neurosurg Psychiatry* 2017;88:575–85. <https://doi.org/10.1136/jnnp-2016-315077>
- [17] Agrawal PB, Joshi M, Marinakis NS, Schmitz-Abe K, Ciarlina PDSC, Sargent JC, et al. Expanding the phenotype associated with the NEFL mutation neuromuscular disease in a family with overlapping myopathic and neurogenic findings. *JAMA Neurol* 2014;71:1413–20. <https://doi.org/10.1001/jamaneurol.2014.1432>
- [18] Tradewell ML, Durham HD, Mushynski WE, Gentil BJ. Mitochondrial and axonal abnormalities precede disruption of the neurofilament network in a model of charcot-marie-tooth disease type 2E and are prevented by heat shock proteins in a mutant-specific fashion. *J Neuropathol Exp Neurol* 2009;68:642–52. <https://doi.org/10.1097/NEN.0b013e3181a5deeb>
- [19] Mul K, Schouten MI, van der Looij E, Dooijes D, Hennekam FAM, Notermans NC, et al. A hereditary spastic paraplegia predominant phenotype caused by variants in the NEFL gene. *Park Relat Disord* 2020;80:98–101. <https://doi.org/10.1016/j.parkreldis.2020.09.016>
- [20] Hashiguchi A, Higuchi Y, Nomura M, Nakamura T, Arata H, Yuan J, et al. Neurofilament light mutation causes hereditary motor and sensory neuropathy with pyramidal signs. *J Peripher Nerv Syst* 2014;19:311–6. <https://doi.org/10.1111/jns.12102>
- [21] Lerat J, Magdelaine C, Beauvais-Dzagan H, Espil C, Ghorab K, Latour P, et al. A novel pathogenic variant of NEFL responsible for deafness associated with peripheral neuropathy discovered through next-generation sequencing and review of the literature. *J Peripher Nerv Syst* 2019;24:139–44. <https://doi.org/10.1111/jns.12310>

- [22] Elbracht M, Senderek J, Schara U, Nolte K, Klopstock T, Roos A, et al. Clinical and morphological variability of the E396K mutation in the neurofilament light chain gene in patients with Charcot-Marie-Tooth disease type 2E. *Clin Neuropathol* 2014;33:335-43. <https://doi.org/10.5414/NP300742>.
- [23] Yuan R, Zhang J, Wang Y, Zhu X, Hu S, Zeng J, et al. Reorganization of chromatin architecture during prenatal development of porcine skeletal muscle. *DNA Res* 2021;28(2):dsab003. <https://doi.org/10.1093/dnares/dsab003>.
- [24] Adriaenssens E, Tedesco B, Mediani L, Asselbergh B, Crippa V, Antoniani F, et al. BAG3 Pro209 mutants associated with myopathy and neuropathy relocate chaperones of the CASA-complex to aggregates. *Sci Rep* 2020;10(1):8755. <https://doi.org/10.1038/s41598-020-65664-z>.
- [25] Massana Muñoz X, Buono S, Koebel P, Laporte J, Cowling BS. Different *in vivo* impacts of dynamin 2 mutations implicated in Charcot-Marie-Tooth neuropathy or centronuclear myopathy. *Hum Mol Genet* 2019;28:4067-77. <https://doi.org/10.1093/hmg/ddz249>.
- [26] Böhm J, Biancalana V, DeChene ET, Bitoun M, Pierson CR, Schaefer E, et al. Mutation spectrum in the large gtpase dynamin 2, and genotype-phenotype correlation in autosomal dominant centronuclear myopathy. *Hum Mutat* 2012;33:949-59. <https://doi.org/10.1002/humu.22067>.
- [27] Pejaver V, Byrne AB, Feng BJ, Pagel KA, Mooney SD, Karchin R, et al. Calibration of computational tools for missense variant pathogenicity classification and ClinGen recommendations for PP3/BP4 criteria. *Am J Hum Genet* 2022;109:2163-77. <https://doi.org/10.1016/j.ajhg.2022.10.013>.
- [28] Richards S, Aziz N, Bale S, Bick D, Das S, Gastier-Foster J, et al. Standards and guidelines for the interpretation of sequence variants: A joint consensus recommendation of the American College of Medical Genetics and Genomics and the Association for Molecular Pathology. *Genet Med* 2015;17:405-24. <https://doi.org/10.1038/gim.2015.30>.
- [29] Mirdita M, Schütze K, Moriwaki Y, Heo L, Ovchinnikov S, Steinegger M. ColabFold: Making protein folding accessible to all. *Nat Methods* 2022;19:679-82. <https://doi.org/10.1038/s41592-022-01488-1>.
- [30] Shao C, Bittrich S, Wang S, Burley SK. Assessing PDB macromolecular crystal structure confidence at the individual amino acid residue level. *Structure* 2022;30:1385-94.e3. <https://doi.org/10.1016/j.str.2022.08.004>.
- [31] Griffith AR, Rogers CJ, Miller GM, Abrol R, Hsieh-Wilson LC, Goddard WA. Predicting glycosaminoglycan surface protein interactions and implications for studying axonal growth. *Proc Natl Acad Sci U S A* 2017;114:13697-702. <https://doi.org/10.1073/pnas.1715093115>.
- [32] Chen Y, Lu H, Zhang N, Zhu Z, Wang S, Li M. PremPS: Predicting the impact of missense mutations on protein stability. *PLoS Comput Biol* 2020;16(12):e1008543. <https://doi.org/10.1371/journal.pcbi.1008543>.
- [33] Dubowitz V, Sewry C, Oldfors A. *Muscle Biopsy. A Practical Approach*. 4. Saunders, London; 2013.
- [34] Katona I, Weis J, Hanisch F. Glycogenosome accumulation in the arrector pili muscle in Pompe disease. *Orphanet J Rare Dis* 2014;9:17. <https://doi.org/10.1186/1750-1172-9-17>
- [35] Hentschel A, Czech A, Münchberg U, Freier E, Schara-Schmidt U, Sickmann A, et al. Protein signature of human skin fibroblasts allows the study of the molecular etiology of rare neurological diseases. *Orphanet J Rare Dis* 2021;16:73. <https://doi.org/10.1186/s13023-020-01669-1>
- [36] Roos A, Preusse C, Hathazi D, Goebel HH, Stenzel W. Proteomic profiling unravels a key role of specific macrophage subtypes in sporadic inclusion body myositis. *Front Immunol* 2019;10:1040. <https://doi.org/10.3389/fimmu.2019.01040>
- [37] Laššuthová P, Šafka Brožková D, Krútová M, Neupauerová J, Haberlová J, Mazanec R, et al. Improving diagnosis of inherited peripheral neuropathies through gene panel analysis. *Orphanet J Rare Dis* 2016;11:118. <https://doi.org/10.1186/s13023-016-0500-5>
- [38] Jordanova A, De Jonghe P, Boerkoel CF, Takashima H, De Vriendt E, Ceuterick C, et al. Mutations in the neurofilament light chain gene (NEFL) cause early onset severe Charcot-Marie-Tooth disease. *Brain* 2003;126:590-7. <https://doi.org/10.1093/brain/awg059>
- [39] Chao HC, Hsiao CT, Lai KL, Tsai YS, Lin KP, Liao YC, et al. Clinical and genetic characterization of NEFL-related neuropathy in Taiwan. *J Formos Med Assoc* 2023;122:132-8. <https://doi.org/10.1016/j.jfma.2022.08.008>
- [40] Carugo O, Pongor S. A normalized root-mean-square distance for comparing protein three-dimensional structures. *Protein Sci* 2008;10:1470-3. <https://doi.org/10.1110/ps.690101>
- [41] Xu X, Zou X. Dissimilar ligands bind in a similar fashion: A guide to ligand binding-mode prediction with application to celpp studies. *Int J Mol Sci* 2021;22(22):12320. <https://doi.org/10.3390/ijms222212320>
- [42] Ramírez D, Caballero J. Is It Reliable to Take the Molecular Docking Top Scoring Position as the Best Solution without Considering Available Structural Data? *Molecules* 2018;23(5):1038. <https://doi.org/10.3390/molecules23051038>
- [43] Cheng JX, Xie XS. Vibrational spectroscopic imaging of living systems: An emerging platform for biology and medicine. *Science* 2015;350(6264):aaa8870350. <https://doi.org/10.1126/science.aaa8870>
- [44] González Coraspe JA, Weis J, Anderson ME, Münchberg U, Lorenz K, Buchkremer S, et al. Biochemical and pathological changes result from mutated Caveolin-3 in muscle. *Skelet Muscle* 2018;8(1):28. <https://doi.org/10.1186/s13395-018-0173-y>
- [45] Rinia HA, Burger KNJ, Bonn M, Müller M. Quantitative label-free imaging of lipid composition and packing of individual cellular lipid droplets using multiplex CARS microscopy. *Biophys J* 2008;95:4908-14. <https://doi.org/10.1529/biophysj.108.137737>
- [46] Benarroch L, Bonne G, Rivier F, Hamroun D. The 2023 version of the gene table of neuromuscular disorders (nuclear genome). *Neuromuscul Disord* 2023;33:76-117. <https://doi.org/10.1016/j.nmd.2022.12.002>
- [47] Lee MK, Marszalek JR, Cleveland DW. A mutant neurofilament subunit causes massive, selective motor neuron death: Implications for the pathogenesis of human motor neuron disease. *Neuron* 1994;13:975-88. [https://doi.org/10.1016/0896-6273\(94\)90263-1](https://doi.org/10.1016/0896-6273(94)90263-1)
- [48] Rossor AM, Sleight JN, Groves M, Muntoni F, Reilly MM, Hoogenraad CC, et al. Loss of BICD2 in muscle drives motor neuron loss in a developmental form of spinal muscular atrophy. *Acta Neuropathol Commun* 2020;8(1):34. <https://doi.org/10.1186/s40478-020-00909-6>
- [49] Issop Y, Hathazi D, Khan MM, Rudolf R, Weis J, Spendiff S, et al. GFPT1 deficiency in muscle leads to myasthenia and myopathy in mice. *Hum Mol*

- Genet 2018;27(18):3218-32. <https://doi.org/10.1093/hmg/ddy225>
- [50] Choi KE, Yim J, Kim M, Lee JH. A Novel HNPP Phenotype in Charcot-Marie-Tooth Type 2E With c.1319C>T Missense Mutation in the NEFL Gene. *J Clin Neurol* 2022;18:244-6. <https://doi.org/10.3988/jcn.2022.18.2.244>
- [51] Petrucci A, Lispi L, Garibaldi M, Frezza E, Moro F, Massa R, et al. Nefl-Related Charcot-Marie Tooth Disease Due To P440I Mutation In Two Italian Families: Expanding The Phenotype And Defining Modulating Factors. *Eur Neurol* 2023;86(3):185-192. <https://doi.org/10.1159/000529706>
- [52] Villegas-Castrejón H, Solís-Arrieta L, Martínez-Flores F, Escobar-Cedillo RE, García-Pérez BE. Peripheral hereditary neuropathies: Charcot-Marie-Tooth types 1 and 2. *Cir Cir* 2004;72.
- [53] Kim HJ, Kim SB, Kim HS, Kwon HM, Park JH, Lee AJ, et al. Phenotypic heterogeneity in patients with NEFL-related Charcot-Marie-Tooth disease. *Mol Genet Genomic Med* 2022;10(2):e1870. <https://doi.org/10.1002/mgg3.1870>
- [54] Evgrafov O V., Mersyanova I, Irobi J, Van Den Bosch L V., Dierick I, Leung CL, et al. Mutant small heat-shock protein 27 causes axonal Charcot-Marie-Tooth disease and distal hereditary motor neuropathy. *Nat Genet* 2004;36:602-6. <https://doi.org/10.1038/ng1354>
- [55] Berciano J, Peeters K, García A, López-Alburquerque T, Gallardo E, Hernández-Fabián A, et al. NEFL N98S mutation: Another cause of dominant intermediate Charcot-Marie-Tooth disease with heterogeneous early-onset phenotype. *J Neurol* 2016;263:361-9. <https://doi.org/10.1007/s00415-015-7985-z>
- [56] Miltenberger-Miltenyi G, Janecke AR, Wanschitz J V., Timmerman V, Windpassinger C, Auer-Grumbach M, et al. Clinical and electrophysiological features in Charcot-Marie-Tooth disease with mutations in the NEFL gene. *Arch Neurol* 2007;64:966-70. <https://doi.org/10.1001/archneur.64.7.966>
- [57] Lin KP, Soong BW, Yang CC, Huang LW, Chang MH, Lee IH, et al. The mutational spectrum in a cohort of Charcot-Marie-Tooth disease type 2 among the han Chinese in Taiwan. *PLoS One* 2011;6(12):e29393. <https://doi.org/10.1371/journal.pone.0029393>